Understanding the Molecular Mechanism of the 1,3-Dipolar Cycloaddition between Fulminic Acid and Acetylene in Terms of the Electron Localization Function and Catastrophe Theory

Victor Polo,[a] Juan Andres,*[a] Raquel Castillo,[a] Slawomir Berski,[a, b] and Bernard Silvi[c]

Abstract: The potential-energy profile of the 1,3-dipolar cycloaddition of fulminic acid and ethyne has been investigated theoretically within the framework provided by the electron localization function (ELF) analysis. This has been achieved by carrying out density functional theory (B3LYP approach) calculations using the bonding evolution theory. Eight different domains of structural stability have been identified along the reaction path, as well as the bifurcation catastrophes responsible for the changes in the topology of the system. The analysis provides a chemical description of the reaction mechanism in terms of heterolytic concerted nonsynchronous bond formation: the first four catastrophes enable the simultaneous formation of the C–C bond and a lone pair on the nitrogen atom, whereas the remaining ones lead to the ring closure. The valence basin populations calculated along the reaction path do not support any mechanism involving pentavalent nitrogen. The simulation of the solvent effect, by means of a continuum model, does not indicate any significant difference of the mechanism of reaction between the gas phase and solution.

Keywords: ab initio calculations · bond theory · cycloaddition · ELF (electron localization function) · reaction mechanisms

Introduction

Theoretical descriptions of chemical reactivity are based on concepts derived from the corresponding potential-energy surface (PES). Molecular structures (reactants, products, and possible intermediates) are associated with the minimum positions in the valleys, while the transition structure (TS) is a saddle point of index one on the PES. The energetic aspects of the reaction can be obtained from the energies of these stationary points, that is, the thermodynamic and kinetic parameters can be derived from the relative values of energy between them. Therefore, the standard description of chemical reactivity tends to rely on calculation of the geometries and energies of these stationary points lying on the reaction pathway of a given chemical rearrangement.

Chemical concepts such as those of bonds and lone pairs enable one to adopt a quite different, but nevertheless complementary, point of view. In this case the effort is put into understanding the changes in bonding that occur along the reaction pathway connecting reactants and products through the corresponding TS. For a chemical reaction involving multiple bond breaking and bond formation, the following main questions need to be answered:

1) How do the chemical events (bond breaking/forming processes) occur, that is, do they follow a step-wise or a concerted mehanism?
2) How does the electronic reorganization proceed along the reaction path?
3) How does the electron flow accompanying the chemical rearrangement relate to the bond breaking/forming processes?
4) Does bond breaking and forming take place in the TS region?

To clarify these matters, some attempts have been made to render a quantitative definition of chemical bonding from quantum mechanical observables obtained from first principle calculations; these include the delocalization index[1–3]

[a] Dr. V. Polo, Prof. J. Andres, Dr. R. Castillo, Dr. S. Berski
Departament de Ciències Experimentals
Universitat Jaume I, Apartat 224
12080 Castelló (Spain)
Fax: (+34) 964-728-066
E-mail: andres@exp.uji.es

[b] Dr. S. Berski
Faculty of Chemistry
University of Wroclaw, F. Joliot-Curie 14
50-383 Wroclaw (Poland)

[c] Prof. B. Silvi
Laboratoire de Chimie Théorique
Université Pierre et Marie Curie, 4 Place Jussieu
75252 Paris Cedex (France)

Supporting information for this article is available on the WWW under http://www.chemeurj.org/ or from the author.

 DOI: 10.1002/chem.200400161

based on the electron pair density in the atoms in molecules (AIM) approach of Bader,[4,5] and a bond basin population from the electron localization function (ELF) approach of Becke and Edgecombe,[6] as extensively developed by Silvi and Savin.[7–15] In particular, the ELF approach is topological and divides a system's space into basins and basin attractors based on the gradients of particular scalar fields. ELF basins are defined quantities although based on strong physical arguments regarding the Fermi hole[16,17] and the corresponding tendency of electron pairs to occupy different regions of space.

In addition, Thom's catastrophe theory is an attempt to find a universal mathematical treatment of morphogenesis,[18] understood as a temporally stable change in the form of a system. We have recently combined ELF and catastrophe theory to analyze the molecular changes that take place along the reaction pathway for the molecular mechanism of the Diels–Alder reaction between ethylene and 1,3-butadiene.[19] The ELF analysis was performed from the Kohn–Sham orbitals for each point along the reaction path and the study of the evolution of ELF basins enabled us to identify the turning points at which there is a change in the number or type of ELF basins. Catastrophe theory is used for an exact characterization of those points. ELF basins can be assigned to electron pairs and the evolution of ELF basins is related to the formation/breaking of chemical bonds or creation/annihilation of lone pairs.[19]

1,3-Dipolar cycloadditions may share features with the more well-known Diels–Alder reaction and since their introduction by Huisgen in 1960,[20,21] the 1,3-dipolar cycloaddition has emerged as a powerful tool in organic synthesis. The five-membered rings formed through 1,3-dipolar cycloadditions are important intermediates in the preparation of natural products, such as alkaloids and β-amino acids.[22–24] In recent times, significant advances have been made in our understanding of these types of cycloadditions, by means of experiments and computational quantum mechanical calculations.[25–27] The mechanism of this type of chemical reaction has been the subject of intense study, but, nevertheless, many of the crucial mechanistic features, such as the direction of the electron flow along the corresponding reaction pathway, remain disputed.[28–34] In this paper, the joint use of ELF analysis and catastrophe theory is applied to a simple 1,3-dipolar cycloaddition reaction between fulminic acid and acetylene.

Computational Methods

Technically, the ELF analysis was performed for a series of structures calculated along the reaction path. The turning points between structural stability domains were then located and the catastrophe identified when the two successive domains belong to the same Born–Oppenheimer energy surface. The calculations were performed by means of density functional theory (DFT) with the B3LYP exchange-correlation potential[35–37] together with the 6–31G(d,p) basis set[38] as included in the Gaussian 98 program.[39] Stationary points on the potential energy surface were confirmed by calculation of harmonic vibrational frequencies, all positive for a minimum and one imaginary for a transition structure (TS). The intrinsic reaction coordinate (IRC) method of Fukui,[40] developed by Gonzalez and Schlegel,[41] was employed to follow the reaction path in mass-weighted coordinates in the forward and reverse directions starting at the TS. Analytical calculation of force constants was performed for each point along the IRC in the gas phase and only at the TS in the solvent phase. The calculated reaction path comprises a total of 140/125 points in the gas/solvent phase with a step size of 0.1 $amu^{1/2}$ Bohr. The topological analysis of ELF was carried out with the TopMod[42] suite and graphical representation by the Amira program.[43] The ELF function was calculated over a rectangular box by using a cubic grid of step size smaller than 0.1 Bohr. The effect of the solvent was simulated by the continuum model of Rivail,[44] based on the use of cavities and a multipolar expansion of the solute electrostatic potential.

What ELF analysis can tell us about the reaction mechanism: The topological analysis of the ELF gradient field, $\nabla\eta(\mathbf{r})$, provides a mathematical model permitting the partition of the molecular position space into basins of attractors, which present in principle a one-to-one correspondence with local chemical objects such as bonds and lone pairs. These basins are either core basins, labeled C(A), or valence basins, V(A,…), belonging to the outermost shell and characterized by their coordination number with core basins; this is called the synaptic order. Very recently[15] it has been demonstrated that the size-independent spin-pair composition function has a clear meaning as a local indicator of chemical bonding, which enables the recovery of the ELF of Becke and Edgecombe. This method has been well documented in a series of articles presenting its theoretical foundations,[6–9,15,45–48] its applications to the understanding of the chemical structure of molecules and solids,[10,11,49–60] the prediction of reactivity,[13,61–66] and the study of chemical reactions in terms of elementary catastrophes.[12,14,19,67–70]

Within the framework provided by the ELF analysis, a chemical reaction is viewed as a series of topological changes occurring along the reaction path. The parameters defining the reaction pathway (such as the nuclear coordinates and the electronic state) constitute the control space. The evolution of the bonding along the reaction path is modeled by the changes in the number and synaptic orders of the valence basins. Each structure is only possible for values of the control parameters belonging to definite ranges, in other words to subsets called structural stability domains (SDD). For any two points of the control space belonging to a given structural stability domain, there is the same number of critical points of each type in the ELF gradient field. Within a structural stability domain, the critical points (i.e., points at which $\nabla\eta(\mathbf{r})=0.0$) are said to be hyperbolic, that is, without zero critical exponent. At the turning points between two consecutive SDDs, at least one critical exponent must be zero in order to change its sign. The type of a critical point is given by the number of positive critical exponents (the positive eigenvalues of the Hessian matrix for a gradient dynamic system) of the critical point. This is called the index I_p. Along the reaction path the chemical system goes from one structural stability domain to another by means of bifurcation catastrophes occurring at the turning points. Each catastrophe transforms the overall topology in such a way that the Poincare–Hopf relation is fulfilled. This technique shows how the bonds are formed and broken and also emphasizes the importance of the geometrical constraints in a chemical reaction. Moreover, the identification of the elementary catastrophe, and therefore the knowledge of its universal unfolding, yields the dimension of the active control space governing the reaction.

From a quantitative viewpoint, the evolution of the total and spin-basin populations along the path provides a key to understanding the role played by the different chemical interactions. Three types of bifurcation catastrophes have been encountered in the study of chemical reactions:

1) The fold catastrophe, which corresponds to the creation or to the annihilation of two critical points of different parity; for example, a wandering point gives rise to an attractor (index 0) and a saddle point of index 1.
2) The cusp catastrophe, which transforms one critical point into three (and vice versa), such as in the formation or the breaking of a covalent bond.
3) The elliptic umbilic catastrophe, in which the index of a critical point changes by two.

Results and Discussion

What can be predicted from the isolated species?: The topology of the ELF function of the fulminic acid molecule reveals four valence basins, namely $V(H_1,C_1)$, $V(C_1,N)$, V(N,O), and V(O), the populations of which are 2.46, 5.73, 1.98, and 5.42 e, respectively. Due to the axial symmetry of the molecule, the attractors of the $V(C_1,N)$ and V(O) basins are degenerated in circles and therefore correspond to structural instabilities, as any lowering of the symmetry would split each circle into several point attractors. The basin populations correspond neither to the standard Lewis structure **1** nor to **2** (Scheme 1), because the population of $V(H_1,C_1)$

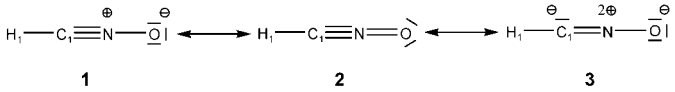

Scheme 1. Proposed resonance structures for fulminic acid **1**–**3**.

is significantly larger than 2.00 e, in fact $\bar{N}[V(H_1,C_1)] = 2.46$ e. In order to model the density distribution by the superposition of resonance forms, structures involving a lone pair on the carbon atom, such as **3**, have to be taken into account.

The populations and number of electrons for each Lewis resonance structure **1**–**3** are reported in Table 1. Structure **1**

Table 1. Basin populations ($\bar{N}$), variance of the basins (σ^2), and number of electrons per basin of the resonance structures.

	ELF			Lewis structures		
	$\bar{N}$	scaled $\bar{N}$[a]	σ^2	**1**	**2**	**3**
$V(H_1,C_1)$	2.46	2.52	0.79	2	2	4
$V(C_1,N)$	5.73	5.88	1.68	6	6	4
V(N,O)	1.98	2.03	1.23	2	4	2
V(O)	5.42	5.56	1.34	6	4	6

[a] The scale factor is 16.0/15.59 = 1.0263.

is in better agreement with the basin populations and with the octet rule, while **2** shows a pentavalent environment for N, and **3** considers the lone pair at C_1 suggested by the high population of $V(H_1,C_1)$. It is possible to calculate the relative weights of the resonance structures, w_1, w_2, and w_3, by solving the following system of nonequivalent linear equations [Eqs. (1)–(5)].

$$w_1 + w_2 + w_3 = 1 \quad (1)$$

$$2w_1 + 2w_2 + 4w_3 = 2.52 \quad (2)$$

$$6w_1 + 6w_2 + 4w_3 = 5.88 \quad (3)$$

$$2w_1 + 4w_2 + 2w_3 = 1.42 \quad (4)$$

$$6w_1 + 4w_2 + 6w_3 = 5.56 \quad (5)$$

Note that the solution depends on the equations considered; a reasonable agreement between calculated and estimated coefficients is 0.72, 0.08, and 0.20 for structures **1**, **2**, and **3**, respectively.

The validity of this model can be checked by the simulation of the δ HCN bending mode (see Scheme 2), which corresponds largely to a vibration calculated at 216 cm^{-1}.

Scheme 2. Bending of HCN angle (δ).

In terms of hybridization we expect that the sp^2 character of the carbon will increase as the angle H_1C_1N decreases from 180° to 120°. The expected trend is already verified for $H_1C_1N = 170°$: the population of the $V(C_1,N)$ and $V(H_1,C_1)$ basins are lowered by 0.34 and 0.11 e, respectively, and a monosynaptic basin $V(C_1)$ appears as shown on Figure 1.

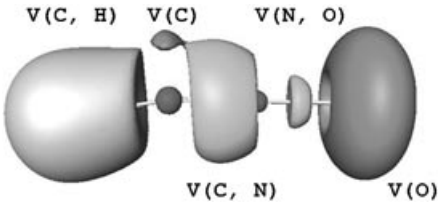

Figure 1. ELF localization domains ($\eta = 0.75$ isosurface) of fulminic acid for $\sphericalangle HCN = 170°$.

The population of this last basin is calculated to be $\bar{N}[V(C_1)] = 0.64$ e. It is worth noting that the cost of this deformation is only 48 cm^{-1}, that is, less than the contribution of ν_1 to the zero-point energy. This $V(C_1)$ basin is the germ of the formation of a bond with ethyne provided another V(C) monosynaptic basin is formed on the ethyne carbon atom. This occurs for the $H_2C_2C_3$ angle of approximately 150° (the energy cost is 9 kcal mol^{-1}). Accordingly, the first step of the cycloaddition will yield an intermediate, for which possible structures are **4** and **5**. Structure **4** does not lead to the final product, whereas structure **5** does by the formation of a dative bond between O and C_2.

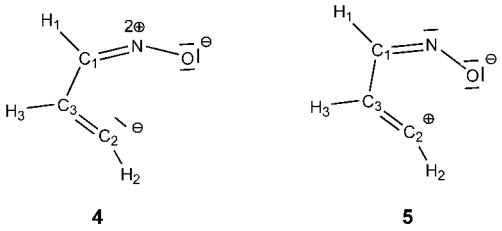

4 **5**

Description of the 1,3-dipolar cycloaddition reaction using ELF and catastrophe theory: In the literature, the 1,3-dipolar cycloaddition reaction of fulminic acid and acetylene has been studied extensively by means of ab initio and DFT methods, leading to an activation energy at the CASPT2//CASSCF(6,6)/6–31G(d) level of 12.2 kcal mol^{-1}[28] and a reaction energy of 77.7 kcal mol^{-1}[45] at the MP4(SDTQ)/6–

311G(d,p)//HF/6–311G(d,p) level. Our study, which makes use of the B3LYP6–31G(d,p) method, gives an activation energy of 13.73 kcal mol^{-1} and an exothermic reaction energy of 78.40 kcal mol^{-1}, including zero-point energy (ZPE) correction in the gas phase (Table 2).

Table 2. Total energies, zero-point-energy, and lowest frequency calculated at the B3LYP6–31G(d,p) level in the gas and solvent phases (total energy only).

	Symmetry	Total energy [au]		ZPE [au]	lowest frequency [cm^{-1}]
		gas	solvent		
HCNO	$C_{\infty v}$	−168.57377	−168.57891	0.01999	217.36
HCCH	$D_{\infty h}$	−77.32957	−77.33247	0.02673	564.39
RC	C_s	−245.90762	−245.91013[a]	0.04780	20.46
TS	C_s	−245.88383	−245.88922	0.04910	−445.28
isoxazole	C_s	−246.03963	−246.04580	0.05808	606.36

[a] Energy corresponding to the first point along the IRC.

Prior to the calculated part of the IRC, fulminic acid and acetylene form a hydrogen-bond complex (reaction complex, RC) in which one hydrogen atom of acetylene points towards the O atom of fulminic acid at an equilibrium distance of 2.260 Å in the gas phase. There is no structural change in the ELF basins relative to the isolated reactants; the stabilization energy of the complex is about 2 kcal mol^{-1} in the gas phase. Geometries for isolated reactants, TS, and isoxazole are presented in Figure 2, optimized for B3LYP6–31G(d,p) in the gas and acetonitrile phases. Solvation does not change the ELF/catastrophe theory description of the reaction considerably. The position and length of steps change slightly, but the sequence and the overall description remains constant. Therefore, in the discussion we will analyze the data for the gas phase. (See supporting information for data for the solvent phase.)

The reaction path calculated at the B3LYP6–31G(d,p) level in the gas phase using the IRC method is shown in Figure 3. A schematic representation of the ELF basins created at each step is depicted below the graph. Calculations were performed by means of ab initio methods; in particular many-body perturbation theory based on the second-order Møller–Plesset perturbation operator (MP2)[72] with the same basis set giving similar results. In order to ensure the stability of the restricted B3LYP wavefunction, stability calculations were carried out for all points along the reaction path.[73] The ELF topology evolution along the reaction path involves eight structural stability domains connected by turning points at which bifurcation catastrophes occur.

The populations for each basin at the turning points between consecutive SDDs are presented in Table 3. For completeness, the ELF analysis for isolated reactants (acetylene and fulminic acid) and the product (isoxazole) are included, as well as the initial point calculated on the IRC path. Distances between atoms C_1–C_3 and C_2–O are also included in the table. The population of core basins remains constant along the reaction path at 10.48 electrons.

The first catastrophe is of fold-type in Thom's catastrophe classification and occurs for $r(C_1–C_3) = 3.213$ Å and $r(C_2–O) = 2.942$ Å. This is a typical plyomorphic process in which the number of basins increases from 11 to 12. The monosynaptic attractor $V(C_1)$ is formed as a result of the deformation of the fulminic acid moiety. Fulminic acid is a 1,3-dipole and strongly polarizes the π-electron cloud of acetylene. Both reactants are parallel to each other to maximize this interaction. During this step, polarization is improved by the bending of the C_1–N–O atoms and leads to a slight zig-zag conformation of H_1C_1NO. The carbon atom deviates from a pure sp hybridization and an electron pair is formed to fill the vacancy at the carbon atom. This is the longest step on the reaction path running over 32 points, while the total energy rises by 8.01 kcal mol^{-1}. Since the universal unfolding of a fold catastrophe depends upon a unique parameter, the dimen-

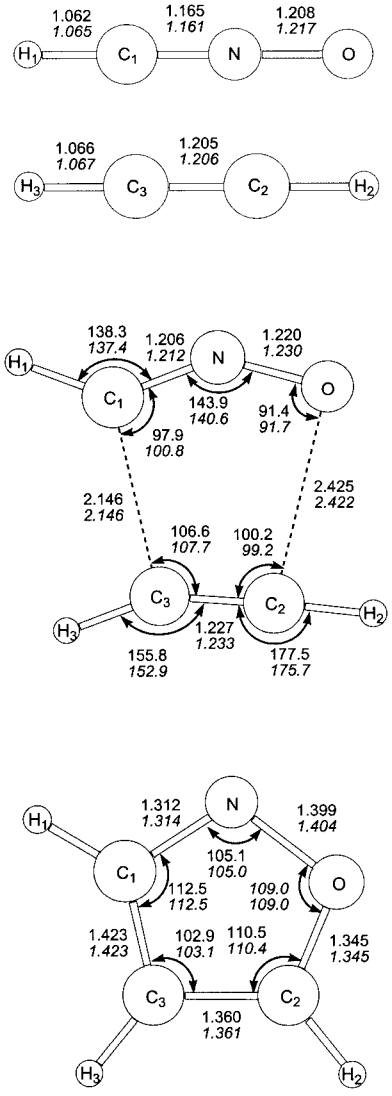

Figure 2. Optimized geometries calculated using B3LYP6–31G(d,p) in the gas (normal) and solvent (italic) phases for isolated reactants, TS, and isoxazole. Bond lengths and bond angles are given in Ångstroms and degrees, respectively.

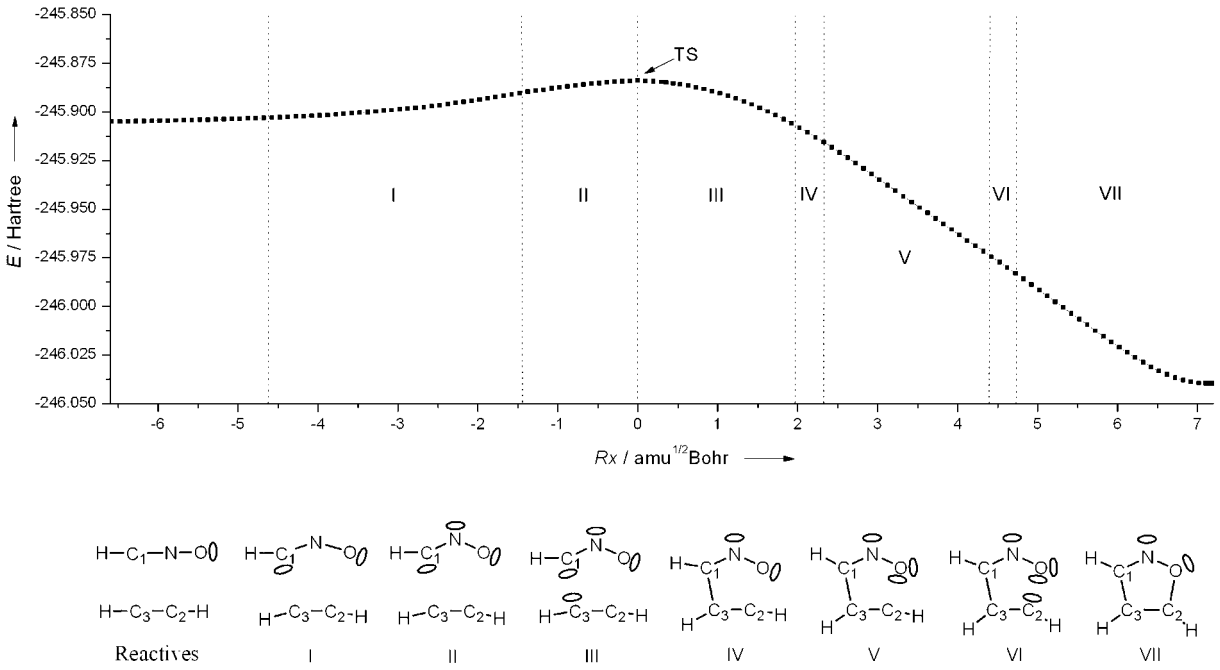

Figure 3. Part of the reaction path studied by means of the IRC method for the reaction between fulminic acid and acetylene in the gas phase. There are, in total, 140 points calculated with a step size of 0.1 amu$^{1/2}$ Bohr. The scheme below the graph shows the ELF basins for each step: a line connecting two atoms means they are connected by one disynaptic (or hydrogenated) basin, while an ellipse means a monosynaptic valence basin attached to the nearest atom.

Table 3. The basin populations ($\bar{N}$) calculated for the ELF basins in the fulminic acid and ethyne reaction in the gas phase, corresponding to different points on the reaction path: isolated reactants, initial point of the IRC, turning points, and product.

Basin	Reactives	Initial point	Step I	Step II	Step III	Step IV	Step V	Step VI	Step VII	Product
	r_{C-C}	3.632	3.213	2.529	2.224	1.852	1.783	1.507	1.489	1.424
	r_{C-O}	3.084	2.942	2.586	2.425	2.216	2.172	1.859	1.802	1.345
$V(C_1)$	–	–	0.20	1.28	1.08					
$V(C_1,C_3)$	–	–	–	–	–	1.43	1.58	2.13	2.17	2.43
$V(C_3)$	–	–	–	–	0.13					
$V(C_1,N)$	5.63	6.06	5.84	3.95	3.51	3.70	3.57	3.14	3.09	2.81
V(N)	–	–	–	1.10	1.90	2.43	2.52	2.84	2.87	3.16
V(N,O)	2.05	1.61	1.63	1.58	1.47	1.33	1.34	1.22	1.20	1.05
$V_1(O)$	5.48	5.64	5.64	5.60	5.62	5.58	5.55	5.24	5.11	4.37
$V_2(O)$	–	–	–	–	–	–	–	0.31		
$V(C_2,O)$	–	–	–	–	–	–	–	–	0.74	1.72
$V(C_2)$	–	–	–	–	–	–	0.12	0.30		
$V(C_2,C_3)$	5.23	5.41	5.34	5.31	5.05	4.34	4.22	3.86	3.84	3.46
$V(H_1,C_1)$	2.47	2.37	2.37	2.19	2.16	2.14	2.15	2.15	2.15	2.15
$V(H_2,C_2)$	2.29	2.21	2.24	2.26	2.30	2.43	2.33	2.22	2.21	2.19
$V(H_3,C_3)$	2.29	2.19	2.24	2.24	2.25	2.14	2.12	2.11	2.11	2.15

sion of the active control space is one. The active control parameter is the angle H_1C_1N bending. A comparison of basin populations at the first point of step I with the isolated reactants reveals the increment of electron density at the lone pairs of the O atom. The basin which represents the lone pairs at this atom, V(O), increases its population from 5.48 to 5.64 e, while $\bar{N}$[V(N,O)] decreases from 2.05 to 1.63 e.

Step II runs over 15 points on the reaction path. There is an increment in the energy of 4.14 kcal mol^{-1} and the step finishes exactly before the TS is reached. The distance $r(C_1–C_3)$ shortens from 2.529 to 2.276 Å, while $r(C_2–O)$ varies from 2.586 to 2.453 Å. There is a change in the $r(C_1–N)$ distance from 1.180 to 1.201 Å; the angle $N–C_1–H_1$ bends from 148.5 to 139°. The catastrophe is of fold type and results in the creation of a monosynaptic basin on the nitrogen atom: V(N). The formation of the lone pair at the N atom reduces its partial positive charge originated by the strong polarization of the N–O bond; this is reflected in the very small population of the V(N,O) basin (1.58 e). To analyze the hierarchical structure of ELF basins when a new chemical entity is created, we have plotted the tree-reduction diagram of the first point of step II in Figure 4 (top). The newly created basin V(N) is connected to $V(C_1,N)$ and to V(N,O) by critical points of index 1 with ELF values 0.83 and 0.70, respectively. Note that the value of V(N) attractor is 0.84, so V(N) and $V(C_1,N)$ are closely joined. The order of steps I and II

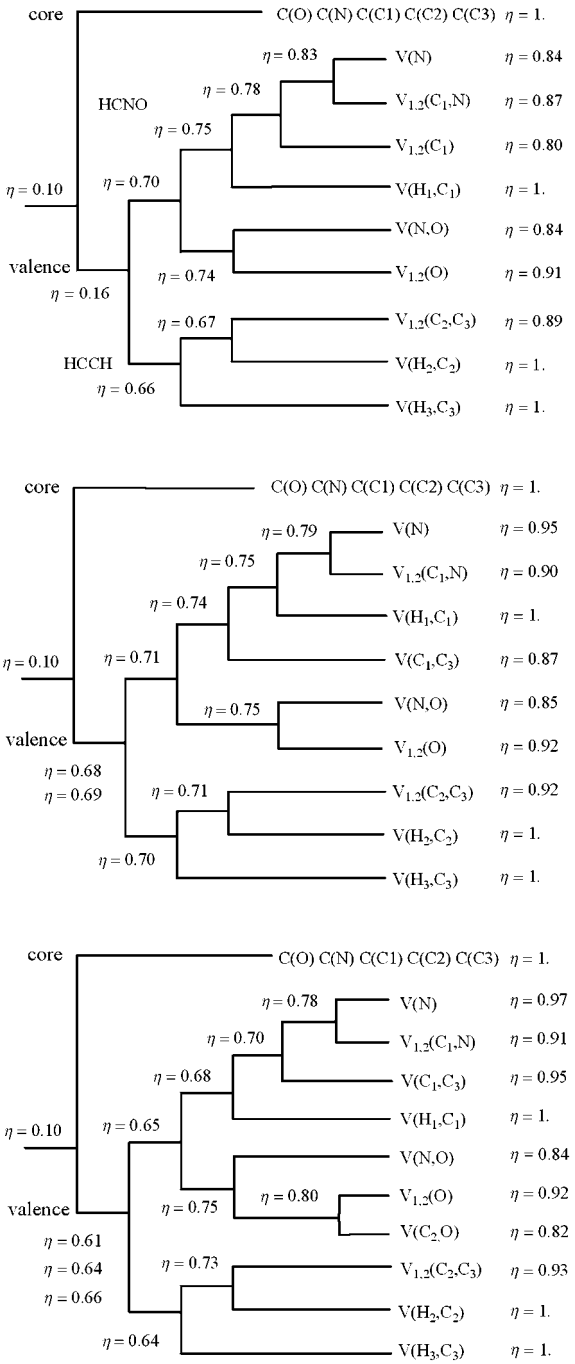

Figure 4. Localization domain tree-reduction diagrams for steps II (top), IV (middle), and VII (bottom) turning points.

is explained by the different flexibility of H_1–C_1–N and C_1–N–O angles. The energy barrier to move the hydrogen from the linear form is lower than for the oxygen and the deviation from linearity leads to the formation of monosynaptic basins $V(C_1)$ and V(N).

The third step starts exactly at the point where the TS is reached and it is characterized by a fold-type catastrophe similar to the one in step I. The monosynaptic $V(C_3)$ basin is formed. The carbon atom C_3 of acetylene "feels" the partial positive charge on C_1 of fulminic acid and accumulates electron density pointing to C_1, while C_3 adopts sp^2 hybridization. In this step changes in the population of other basins are involved: $V(C_1,N)$ and $V(C_2,C_3)$ decrease and $V(C_1)$, V(N), and $V(C_3)$ increase. There is a concentration of electron density in the region between C_1 and C_3 as a prelude of the formation of the C_1–C_3 covalent bond along the next step. At this point, the distance $r(C_1$–$C_3)$ (2.224 Å) is shorter than $r(C_2$–O) (2.425 Å); the angle $H_3C_3C_2$ is 155.8°. Step III runs over 20 points and the energy lowers by 13.95 kcal mol^{-1}. Figure 5c shows the ELF basins at the TS.

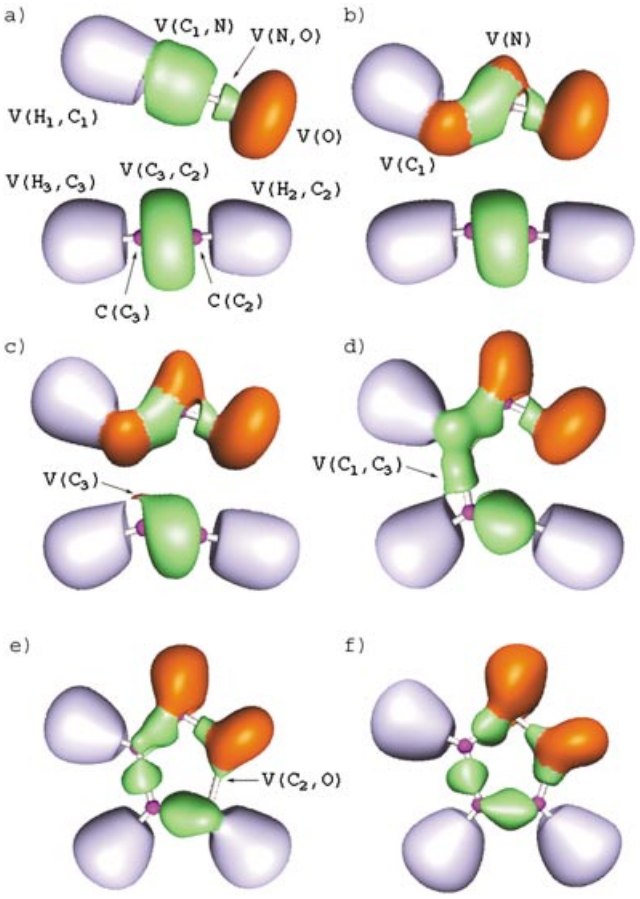

Figure 5. Snapshots of ELF localization domains ($\eta = 0.71$ isosurface) for a) reactants, b) step II turning point, c) TS, d) step IV turning point, e) step VII turning point, and f) product.

The fourth step is characterized by a cusp catastrophe. Two monosynaptic basins $V(C_1)$ and $V(C_3)$ disappear to form a disynaptic basin $V(C_1,C_3)$, representing the formation of the C_1–C_3 covalent bond. The distance $r(C_1$–$C_3)$ is 1.852 Å and $r(C_2$–O) is 2.216 Å. This step runs over only 4 points and the energy decreases by 6.02 kcal mol^{-1}. The tree-reduction bifurcation diagram is plotted in Figure 4 (middle). The newly created basin $V(C_1,C_3)$ possess a maximum ELF value of 0.87 and it is connected to $V_{1,2}(C_1,N)$ and $V_{1,2}(C_2,C_3)$ by critical points of index 1 with ELF values of 0.74 and 0.68, respectively. Looking at the populations, $\bar{N}[V(C_1,N)]$ increases sharply up to 0.88 e while the $\bar{N}[V(C_2,C_3)]$ remains constant. The basin $V(C_1)$ in the previous steps has borrowed electron density from $V(C_1,N)$ to improve polarization forces between fulminic acid and acetylene, and once the chemical bond C_1–C_3 is formed, the

electron density borrowed previously returns quickly to the $V(C_1,N)$ basin.

The next catastrophe happens at $r(C_1–C_3)=1.783$ Å and $r(C_2–O)=2.172$ Å. It is a fold-type catastrophe and the number of basins increases from 13 to 14. After the $C_1–C_3$ bond is formed, the population of $V(C_2–C_3)$ decreases, loosing the triple-bond character. The carbon C_2 is almost sp^2 hybridized and a small quantity of electron density forms $V(C_2)$. The population of $V(C_2)$ starts with 0.13 e and the maximum population reached is 0.50 e, revealing a large positive charge at C_2 during this step. Other basins suffer important variations in their population during this step: $V(C_1,N)$ and $V(C_2,C_3)$ decrease, while V(N) and $V(C_1,C_3)$ increase to reach a population closer to a typical lone pair and a single bond. Step V runs over 21 points and the energy decreases by 36.97 kcal mol^{-1}.

The sixth catastrophe occurs for $r(C_1–C_3)=1.507$ Å and $r(C_2–O)=1.859$ Å. It is a fold catastrophe and the number of basins increases from 15 to 16. Step VI is similar to steps I, III, and V, and a monosynaptic basin $V_2(O)$ is formed. There are two basins $V_1(O)$ and $V_2(O)$ corresponding to the lone pairs on the O atom, but the new one, $V_2(O)$, is much less populated. The large electronegativity of the O atom impedes the sharing of electron density from its lone pairs, but finally the partial positive charge at C_2 leads to the formation of $V_2(O)$ pointing towards C_2. This is the shortest step, just 3 points along the reaction path and the energy decreases by 5.35 kcal mol^{-1}.

The last step is determined by the seventh catastrophe, running over 27 points along the reaction path. The catastrophe results in the formation of the $C_2–O$ bond. In Thom's classification the catastrophe belongs to a cusp type. Two monosynaptic basins, $V_2(O)$ and $V(C_2)$, collapse into a new disynaptic basin $V(C_2,O)$. The associated process is of the miomorphic type and the number of basins decreases from 16 to 15. This step is interpreted as the closure of the ring. The distance $r(C_2–O)$ is still long (1.826 Å) but a disynaptic basin $V(C_2,O)$ has been formed. In Figure 4 (bottom), the topology of the ELF is studied by the tree-reduction diagram of ELF basins at the first point of step VII. The maximum ELF of the new basin $V(C_2,O)$ is $\eta=0.82$ and it is connected to $V_1(O)$ and $V_{1,2}(C_2,C_3)$ by critical points of index 1, with ELF values $\eta=0.80$ and 0.61, respectively. The very different population of $V_1(O)$ (5.55 e) and $V(C_2)$ (0.30 e) prior to the bond formation suggests a bonding of dative type between the lone pair of O and the positively charged C_2. The step lasts for 27 points on the IRC; the energy decreases by 35.47 kcal mol^{-1} until the minimum is found.

The IRC path concludes when the minimum corresponding to the isoxazole molecule is found. The population of the newly created basins along the reaction course presents maximal value at the product of $V(C_1,C_3)=2.43$ e, $V(C_2,O)=1.72$ e, and $V(N)=3.16$ e. On the other hand, the rest of the basins possess minimal populations: $V(C_2,C_3)=3.46$ e, $V(C_1,N)=2.81$ e, $V(N,O)=1.05$ e, and $V(O)=4.37$ e. It is interesting to compare the populations of $V(C_2,O)$ (1.72 e) and V(N,O) (1.05 e). A typical single C–C bond is represented by a disynaptic bond basin possessing a population around 1.9 e. The presence of an electronegative atom (O) decreases the bond basin population and attracts the bond basin towards the more electronegative atom. In Figure 5, the complete sequence of snapshots of the ELF for the more crucial points along the reaction path is presented.

Conclusions

The ELF and catastrophe theory provide a powerful technique for characterizing the steps of the reaction mechanism for the 1,3-dipolar cycloaddition between fulminic acid and acetylene. This work presents a clear description of the molecular mechanism, which is characterized by seven catastrophes (five fold-type and two cusp-type catastrophes).

The reaction can be viewed as a transfer of electron density from the reactant-like basins into three newly created basins that represent two chemical bonds between the reactants and a lone pair on the N atom in the eight steps characterized by catastrophe theory. Comparing the populations between the reactants and the product, the largest drain of electron density is for the basin $V(C_1,N)$ loosing 2.82 e. Other basins also present a decrement in their population: $V(C_2,C_3)$ 1.76 e, V(O) 1.09 e, and V(N,O) 1.00 e. This electron density is relocated into the new basins formed along the reaction course: $V(C_1,C_3)$, $V(C_2,O)$, and V(N) present maxima of populations at the product of 2.43 e, 1.72 e, and 3.16 e, respectively.

The whole reaction path involves eight structural stability domains. The first step of the reaction leads to the activated complex. It is clearly driven by the low-frequency modes of the reactants that are responsible for the fold catastrophes giving rise to the monosynaptic basins $V(C_1)$, V(N), and $V(C_3)$. The activated complex formation is then obtained through a cusp catastrophe, which merges $V(C_1)$ and $V(C_3)$ into $V(C_1,C_3)$. The ring closure is a dative process in which the oxygen atom provides an electron pair, since it occurs by means of a cusp catastrophe prepared by two fold catastrophes. In fact the total valence population of the oxygen atom decreases after the transition state and is minimal before the closing cusp catastrophe.

The molecular mechanism of a given chemical reaction can be decomposed and characterized by the joint use of ELF analysis and catastrophe theory into a sequence of steps that represent simple chemical changes. It is therefore an appropriate tool in the contemporary understanding of the principles governing chemical reactivity.

Acknowledgments

This work was supported by Universitat Jaume I-Fundacio Bancaixa, Project P1B99–02. The authors thank the Servei d'Informatica, Universitat Jaume I, and the Wroclaw Centre for Networking, and Supercomputing for a generous allotment of computer time. The Marie Curie Development Host Fellowship program supported the work of S.B.—contract No. HPMD-CT-2000–00055. The authors are solely responsible for the information communicated and it does not represent the opinion of The European Community. The European Community is not responsible for any use that might be made of data appearing therein.

[1] X. Fradera, M. A. Austen, R. F. W. Bader, *J. Phys. Chem. A* **1999**, *103*, 304–314.
[2] J. Poater, M. Solá, M. Duran, X. Fradera, *J. Phys. Chem. A* **2001**, *105*, 6249–6257.
[3] J. Poater, M. Solá, M. Duran, X. Fradera, *J. Phys. Chem. A* **2001**, *105*, 2052–2063; corrigendum: J. Poater, M. Solá, M. Duran, X. Fradera, *J. Phys. Chem. A* **2002**, *106*, 4794.
[4] R. F. W. Bader, *Acc. Chem. Res.* **1985**, *18*, 9–15.
[5] R. F. W. Bader, *Atoms in Molecules. A Quantum Theory*, Claredon Press, Oxford, **1990**.
[6] A. D. Becke, K. E. Edgecombe, *J. Chem. Phys.* **1990**, *92*, 5397–5403.
[7] A. Savin, A. D. Becke, J. Flad, R. Nesper, H. Preuss, H. G. von Schnering, *Angew. Chem.* **1991**, *103*, 421; *Angew. Chem. Int. Ed. Engl.* **1991**, *30*, 409–412.
[8] A. Savin, O. Jespen, J. Flad, O. K. Andersen, H. Preuss, H. G. von Schnering, *Angew. Chem.* **1992**, *104*, 186–188; *Angew. Chem. Int. Ed. Engl.* **1992**, *31*, 185–187.
[9] B. Silvi, A. Savin, *Nature* **1994**, *371*, 683–686.
[10] A. Savin, R. Nesper, S. Wengert, T. Fassler, *Angew. Chem.* **1997**, *109*, 1892–1918; *Angew. Chem. Int. Ed. Engl.* **1997**, *36*, 1808–1832.
[11] R. Llusar, A. Beltrán, J. Andrés, S. Noury, B. Silvi, *J. Comput. Chem.* **1999**, *20*, 1517–1526.
[12] X. Krokidis, R. Vuilleumier, D. Borgis, B. Silvi, *Mol. Phys.* **1999**, *96*, 265–273.
[13] F. Fuster, A. Savin, B. Silvi, *J. Comput. Chem.* **2000**, *21*, 509–514.
[14] M. C. Michelini, E. Sicilia, N. Russo, M. E. Alikhani, B. Silvi, *J. Phys. Chem. A* **2003**, *107*, 4862–4868.
[15] B. Silvi, *J. Phys. Chem. A* **2003**, *107*, 3081–3085.
[16] R. McWeeny, *Rev. Mod. Phys.* **1960**, *32*, 335–369.
[17] R. McWeeny, *Methods of Molecular Quantum Mechanics*, 2nd ed., Academic Press, New York, **1989**.
[18] R. Thom, *Structural Stability and Morphogenesis: An Outline of a General Theory of Models*, Benjamin, Reading, **1975**; T. Poston, L. Stewart, *Catastrophe Theory and its Applications*, Dover, Mineola, New York, **1996**.
[19] S. Berski, J. Andrés, B. Silvi, L. R. Domingo, *J. Phys. Chem. A* **2003**, *107*, 6014–6024.
[20] R. Huisgen, *Proc. Chem. Soc. London* **1961**, *357–369*.
[21] A. Padwa, *1,3-Dipolar Cycloaddition Chemistry*, Wiley, New York, **1984**.
[22] K. V. Gothelf, K. A. Jorgensen, *Chem. Rev.* **1998**, *98*, 863–910.
[23] S. Karlsson, H. Högberg, *Org. Prep. Proced. Int.* **2001**, *33*, 103–172.
[24] V. Y. Kukushkin, A. J. L. Pombeiro, *Chem. Rev.* **2002**, *102*, 1771–1802.
[25] K. N. Houk, J. González, Y. Li, *Acc. Chem. Res.* **1995**, *28*, 81–90.
[26] C. D. Valentin, M. Freccero, R. Gandolfi, A. Rastelli, *J. Org. Chem.* **2000**, *65*, 6112–6120.
[27] *Cycloaddition Reactions in Organic Synthesis* (Eds.: S. Kobayashi, K. A. Jorgensen), Wiley-VCH, Weinheim **2001**.
[28] P. B. Karadakov, D. L. Cooper, J. Gerratt, *Theor. Chem. Acc.* **1998**, *100*, 222–229.
[29] M. T. Nguyen, A. K. Chandra, S. Sakai, K. Morokuma, *J. Org. Chem.* **1999**, *64*, 65–69.
[30] R. D. Harcourt, A. Schulz, *J. Phys. Chem. A* **2000**, *104*, 6510–6516.
[31] K. Sakata, *J. Phys. Chem. A* **2000**, *104*, 10001–10008.
[32] M. T. Nguyen, A. K. Chandra, T. Uchimaru, S. Sakai, *J. Phys. Chem. A* **2001**, *105*, 10943–10945.
[33] P. B. Karadakov, D. L. Cooper, *J. Phys. Chem. A* **2001**, *105*, 10946.
[34] R. D. Harcourt, *J. Phys. Chem. A* **2001**, *105*, 10947–10948.
[35] A. D. Becke, *J. Chem. Phys.* **1993**, *98*, 1372–1377.
[36] A. D. Becke, *J. Chem. Phys.* **1993**, *98*, 5648–5652.
[37] C. Lee, W. Yang, R. G. Parr, *Phys. Rev. B* **1988**, *37*, 785–789.
[38] P. C. Hariharan, J. A. Pople, *Theor. Chim. Acta* **1973**, *28*, 213–222.
[39] Gaussian 98, Revision A.9, M. J. Frisch, G. W. Trucks, H. B. Schlegel, G. E. Scuseria, M. A. Robb, J. R. Cheeseman, V. G. Zakrzewski, J. A. Montgomery, R. E. Stratmann, Jr., J. C. Burant, S. Dapprich, J. M. Millam, A. D. Daniels, K. N. Kudin, M. C. Strain, O. Farkas, J. Tomasi, V. Barone, M. Cossi, R. Cammi, B. Mennucci, C. Pomelli, C. Adamo, S. Clifford, J. Ochterski, G. A. Petersson, P. Y. Ayala, Q. Cui, K. Morokuma, D. K. Malick, A. D. Rabuck, K. Raghavachari, J. B. Foresman, J. Cioslowski, J. V. Ortiz, A. G. Baboul, B. B. Stefanov, G. Liu, A. Liashenko, P. Piskorz, I. Komaromi, R. Gomperts, R. L. Martin, D. J. Fox, T. Keith, M. A. Al-Laham, C. Y. Peng, A. Nanayakkara, M. Challacombe, P. M. W. Gill, B. Johnson, W. Chen, M. W. Wong, J. L. Andres, C. Gonzalez, M. Head-Gordon, E. S. Replogle, J. A. Pople, Pittsburgh PA, **1998**.
[40] K. Fukui, *J. Phys. Chem.* **1970**, *74*, 4161–4163; K. Fukui, *Acc. Chem. Res.* **1981**, *14*, 363–368.
[41] C. Gonzalez, H. B. Schlegel, *J. Phys. Chem.* **1990**, *94*, 5223–5227.
[42] S. Noury, X. Krokidis, F. Fuster, B. Silvi, *Comput. Chem.* **1999**, *23*, 597–604.
[43] Amira 3.0, Indeed—Visual Concepts, Berlin, **2003**.
[44] J. L. Rivail, *Chem. Phys.* **1976**, *18*, 233–242; J. L. Rivail, *THEOCHEM* **1985**, *120*, 387–400; J. Rinaldi, *J. Comput. Chem.* **1992**, *13*, 675–680; J. Rinaldi, A. Bouchy, J. L. Rivail, V. Dillet, *J. Chem. Phys.* **2004**, *120*, 2343–2350.
[45] C. Sosa, J. Andzelm, C. Lee, J. F. Blake, B. L. Chenard, T. W. Butler, *Int. J. Quantum Chem.* **1994**, *49*, 511–526.
[46] U. Häussermann, S. Wengert, R. Nesper, *Angew. Chem.* **1994**, *106*, 2150–2154; *Angew. Chem. Int. Ed. Engl.* **1994**, *33*, 2073–2076.
[47] A. Savin, B. Silvi, F. Colonna, *Can. J. Chem.* **1996**, *74*, 1088–1096.
[48] S. Noury, F. Colonna, A. Savin, B. Silvi, *J. Mol. Struct.* **1998**, *450*, 59–68.
[49] B. Silvi, *J. Mol. Struct.* **2002**, *614*, 3–10.
[50] B. Silvi, A. Savin, F. R. Wagner in *Modelling of Minerals and Silicated Materials* (Eds.: B. Silvi, P. D'Arco), Topics in Molecular Organization and Engineering 15, Kluwer Academic, Dordrecht, The Netherlands, **1997**, pp. 179–199.
[51] A. Beltrán, J. Andrés, S. Noury, B. Silvi, *J. Phys. Chem. A* **1999**, *103*, 3078–3088.
[52] F. Fuster, B. Silvi, *Theor. Chem. Acc.* **2000**, *104*, 13–21.
[53] B. Silvi, C. Gatti, *J. Phys. Chem. A* **2000**, *104*, 947–953.
[54] R. Choukroun, B. Donnadieu, J. S. Zhao, P. Cassoux, C. Lepetit, B. Silvi, *Organometallics* **2000**, *19*, 1901–1911.
[55] D. B. Chesnut, L. J. Bartolloti, *Chem. Phys.* **2000**, *253*, 1–11.
[56] D. B. Chesnut, L. J. Bartolloti, *Chem. Phys.* **2000**, *257*, 175–181.
[57] D. B. Chesnut, *J. Phys. Chem. A* **2000**, *104*, 7635–7638.
[58] C. Fressigné, J. Maddaluno, A. Márquez, C. J. Giesner-Prette, *J. Org. Chem.* **2000**, *65*, 8899–8907.
[59] S. Noury, B. Silvi, R. G. Gillespie, *Inorg. Chem.* **2002**, *41*, 2164–2172.
[60] R. G. Gillespie, B. Silvi, *Coord. Chem. Rev.* **2002**, *233*, 53–62.
[61] D. B. Chesnut, *J. Phys. Chem. A* **2003**, *107*, 4307–4313.
[62] F. Fuster, B. Silvi, *Chem. Phys.* **2000**, *252*, 279–287.
[63] F. Fuster, A. Savin, B. Silvi, *J. Phys. Chem. A* **2000**, *104*, 852–858.
[64] M. Oliva, V. S. Safont, J. Andrés, O. Tapia, *Chem. Phys. Lett.* **2001**, *340*, 391–399.
[65] E. Chamorro, J. C. Santos, B. Gómez, R. Contreras, P. Fuentealba, *J. Phys. Chem. A* **2002**, *106*, 11533–11539.
[66] E. Chamorro, A. Toro-Labbe, P. Fuentealba, *J. Phys. Chem. A* **2002**, *106*, 3891–3898.
[67] J. C. Santos, P. Fuentealba, *J. Chem. Phys.* **2004**, *120*, 1670–1673.
[68] X. Krokidis, S. Noury, B. Silvi, *J. Phys. Chem. A* **1997**, *101*, 7277–7282.
[69] X. Krokidis, V. Goncalves, A. Savin, B. Silvi, *J. Phys. Chem. A* **1998**, *102*, 5065–5073.
[70] X. Krokidis, B. Silvi, M. E. Alikhani, *Chem. Phys. Lett.* **1998**, *292*, 35–45.
[71] X. Krokidis, N. W. Moriarty, W. A. Lester, Jr., M. Frenklach, *Chem. Phys. Lett.* **1999**, *314*, 534–542.
[72] C. Møller, M. S. Plesset, *Phys. Rev.* **1934**, *46*, 618–622.
[73] R. Bauernschmitt, R. Ahlrichs, *J. Chem. Phys.* **1996**, *104*, 9047–9052.

Received: February 18, 2004
Published online: September 13, 2004